

DeltaKWS: A 65nm 36nJ/Decision Bio-inspired Temporal-Sparsity-Aware Digital Keyword Spotting IC with 0.6V Near-Threshold SRAM

Qinyu Chen*[✉], Member, IEEE, Kwantae Kim*[✉], Member, IEEE, Chang Gao*[✉], Member, IEEE, Sheng Zhou[✉], Taekwang Jang[✉], Senior Member, IEEE, Tobi Delbruck[✉], Fellow, IEEE, Shih-Chii Liu[✉], Fellow, IEEE

Abstract—This paper introduces DeltaKWS, to the best of our knowledge, the first Δ RNN-enabled fine-grained temporal sparsity-aware Keyword Spotting (KWS) integrated circuit (IC) for voice-controlled devices. The 65 nm prototype chip features a number of techniques to enhance performance, area, and power efficiencies, specifically: 1) a bio-inspired delta-gated recurrent neural network (Δ RNN) classifier leveraging temporal similarities between neighboring feature vectors extracted from input frames and network hidden states, eliminating unnecessary operations and memory accesses; 2) an infinite impulse response (IIR) bandpass filter (BPF)-based feature extractor (FEx) that leverages mixed-precision quantization, low-cost computing structure and channel selection; 3) a 24 kB 0.6 V near- V_{TH} weight static random-access memory (SRAM) that achieves 6.6 \times lower read power than the foundry-provided SRAM. From chip measurement results, we show that the DeltaKWS achieves an 11/12-class Google Speech Command Dataset (GSCD) accuracy of 90.5%/89.5% respectively and energy consumption of 36 nJ/decision in 65 nm CMOS process. At 87% temporal sparsity, computing latency and energy/inference are reduced by 2.4 \times /3.4 \times , respectively. The IIR BPF-based FEx, Δ RNN accelerator, and 24 kB near- V_{TH} SRAM blocks occupy 0.084 mm², 0.319 mm², and 0.381 mm² respectively (0.78 mm² in total).

Index Terms—Keyword spotting (KWS), IC, Near-Threshold SRAM, Infinite impulse response (IIR), Delta-gated recurrent neural network.

I. INTRODUCTION

KEYWORD Spotting (KWS) is an essential always-on function for voice-activated devices. The KWS wakes up the downstream building blocks of the internet of things (IoT) devices by recognizing specific keywords, facilitating ultra-low-power consumption and always-on operation. This area has attracted significant research attention for integrated circuit

(IC) in design community [1]–[8] where the challenge lies in minimizing power consumption while keeping high Keyword Spotting (KWS) accuracy.

Advancements in artificial intelligence (AI) techniques have led to extensive applications of neural network models in KWS classifiers. Models such as convolutional neural networks (CNNs), recurrent neural networks (RNNs), and attention mechanism networks utilize their powerful data mining capabilities to learn and identify keyword-relevant characteristics, resulting in superior accuracy. However, the complexity of these networks leads to redundant computations and increased hardware costs at the edge.

Reported methods to increase the energy efficiency of KWS ICs include exploiting the inherent weight and activation sparsity of the subsequent neural network to reduce redundant computations. KWS chip designs are commonly tested on the Google Speech Command Dataset (GSCD). A recurrent attention in-memory KWS IC exploited activation sparsity but only achieved up to 70% activation sparsity on a 7-class GSCD subset [3]. A switch-capacitor array-based KWS chip used a CNN model as a classifier, and exploited bit-level sparsity in weights and achieved 90.9% accuracy on an 11-class GSCD subset [6]. A KWS system-on-chip (SoC) running skip-RNN exploited 76% coarse-grained temporal sparsity by skipping audio frames but reported only on a 7-class GSCD subset [8]. None have exploited temporal sparsity in the change of neural network activations as an additional method of increasing the energy efficiency of KWS ICs.

Other ICs focused on reducing the power of the audio feature extractor (FEx), commonly employing serial Fast Fourier Transform (FFT)-based or time-domain band-pass filtered features, and using a single deep neural network for both feature extraction and classification. A serial FFT-based KWS chip achieved 510 nW but at the cost of a 64 ms latency in a 2-class GSCD subset [2]. A 23 μ W KWS chip demonstrated an analog ring-oscillator-based time-domain FEx but only achieved around 86% accuracy on the full 12-class GSCD [1]. A single-chip fully synthesizable Wired-Logic deep neural network (DNN) processor [5] used a single 16-layer DNN model for feature extraction and classification; however, it only achieved 88% accuracy for 10 keywords subset. In addition, 40%-to-60% [1], [2], [6] of the total IC power was dominated by weight memory (e.g., static random-access memory (SRAM)), which limits the scaling to larger networks required for real-world applications.

*Equal Contribution.

Qinyu Chen was with the Institute of Neuroinformatics, University of Zürich and ETH Zürich, Switzerland. She is now with the Leiden Institute of Advanced Computer Science (LIACS), Leiden University, The Netherlands.

Kwantae Kim was with the Institute of Neuroinformatics, University of Zürich and ETH Zürich, Switzerland, and also with the Department of Information Technology and Electrical Engineering (D-ITET), ETH Zürich, Switzerland. He is now with the Department of Electronics and Nanoengineering, School of Electrical Engineering, Aalto University, Espoo, Finland.

Chang Gao is with the Department of Microelectronics, Delft University of Technology, The Netherlands.

Taekwang Jang is with the Department of Information Technology and Electrical Engineering (D-ITET), ETH Zürich, Switzerland.

Sheng Zhou, Tobi Delbruck and Shih-Chii Liu are with the Institute of Neuroinformatics, University of Zürich and ETH Zürich, Switzerland.

Corresponding authors: Qinyu Chen (q.chen@liacs.leidenuniv.nl) and Shih-Chii Liu (shih@ini.uzh.ch).

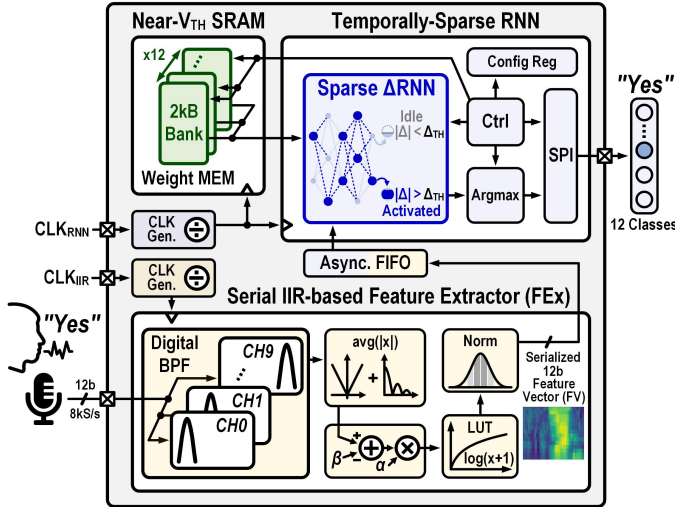


Fig. 1. Overall architecture of proposed temporally-sparse Δ RNN KWS IC with IIR BPF-based time-domain FEx and near- V_{TH} weight SRAM.

We present DeltaKWS, which shows improvements in area and energy efficiency while achieving $> 90\%$ accuracy through the use of the following three key blocks:

- 1) A bio-inspired Δ RNN accelerator leveraging temporal similarities between neighboring feature vectors extracted from input frames and network hidden states, eliminating unnecessary operations and memory accesses; achieving $2.4\times$ latency reduction and $3.4\times$ energy per decision reduction.
- 2) A serial infinite impulse response (IIR)-bandpass filter (BPF) FEx featuring mixed-precision quantization, low-cost computing structure, and channel selection, achieving $5.7\times$ power reduction and $4.7\times$ area reduction.
- 3) A 24 kB 0.6 V near-threshold-operating full-custom SRAM achieving $6.6\times$ lower power consumption.

The proposed KWS chip prototyped in 65 nm CMOS process incorporates an IIR BPF-based FEx, Δ RNN accelerator, and 24 kB near-threshold SRAM, occupying 0.78 mm^2 , with 36 nJ/Decision energy efficiency.

This article is organized as follows. Section II details the bio-inspired temporal sparsity-aware KWS system. Section III reports the system implementation of the always-on KWS task and measurement results. Section IV concludes this article.

II. BIO-INSPIRED TEMPORAL-SPARSITY-AWARE KWS SYSTEM

The details of the DeltaKWS architecture are described first in Section II-A. Section II-B describes the blocks of the Δ RNN accelerator. Section II-C covers the IIR BPF-based FEx, and Section II-D provides information about the near- V_{TH} SRAM.

A. Architectural Overview

Fig. 1 shows the chip architecture with a Δ RNN accelerator, a 24 kB near- V_{TH} SRAM for weight storage, and a compact serial IIR BPF-based time-domain FEx. The input of FEx is 12b

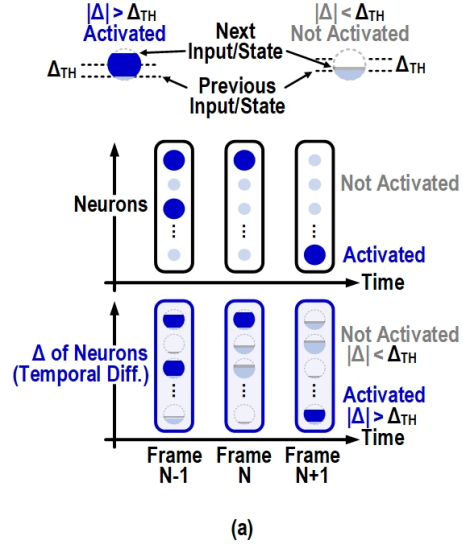


Fig. 2. Concept of Δ network: (a) Δ neurons along time axis. The bottom row illustrates the process by which neuron states are determined across frames in a GRU network, showing the temporal differences that drive these state changes. The middle row shows the resulting neuron states across frames in the GRU network, indicating which neurons are activated (dark blue) or inactivated (light blue) based on these temporal differences. The upper row provides a detailed view, indicating that a neuron is only activated when its temporal difference exceeds the defined threshold. (b) The Δ GRU structure, with 10 input channels, processes data through a Δ RNN layer containing 64 neurons, followed by a fully connected layer that classifies inputs into 12 command categories: ‘Silence,’ ‘Unknown,’ ‘Down,’ ‘Go,’ ‘Left,’ ‘No,’ ‘Off,’ ‘On,’ ‘Right,’ ‘Stop,’ ‘Up,’ and ‘Yes.’ In this work, we also evaluate 11-class accuracy [6], excluding the ‘Unknown’ category.

streamed with a serial peripheral interface (SPI) interface. An asynchronous FIFO connects FEx 12b outputs to the Δ RNN accelerator across various clock domains. Two clock dividers driven by the master clock generated by a field programmable gate array (FPGA) are used to reduce the fast clocks (CLK_{RNN} and CLK_{IIR}) to slower speeds. This is necessary because while SPI transfers 1b per clock cycle and requires a faster clock for interfacing, the processing within the chip operates more efficiently at a slower clock speed. The 24 kB near- V_{TH} SRAM stores the entire Δ RNN model weights. On-chip storing avoids constant off-chip weight access, saving considerable energy ($1 \mu\text{J}$ to read 6.2 kB data from dynamic random-access memory (DRAM) [9]).

B. Temporally Sparse Δ RNN

Neurons in the cerebral cortex exhibit a spiking threshold; their activation is not only discrete over time but also capped

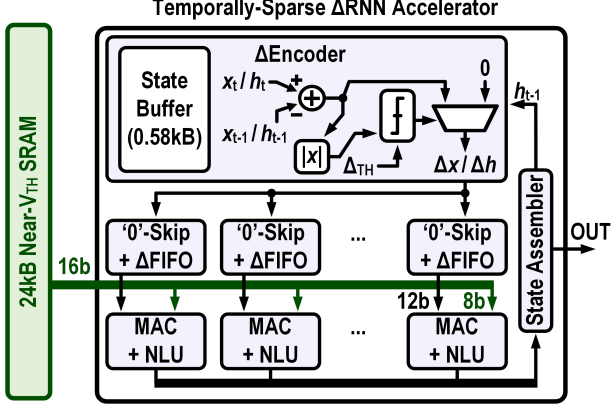


Fig. 3. The architecture of the Δ RNN accelerator. The 24 kB weight memory provides 16 bit words, storing two 8 bit Δ RNN weights.

at a finite firing rate. Inspired by these neuromorphic characteristics, researchers have explored the concept of inducing temporal sparsity in artificial recurrent neural networks. This approach has been termed the Δ RNN model [10]–[14]. Fig. 2 illustrates the concept of the Δ RNN and the architecture for the KWS network. The Δ RNN employs fine-grained temporal sparsity by allowing neurons to update their targets only when their delta change in activation exceeds a defined threshold, thus skipping unnecessary computations and memory accesses. This mechanism can significantly boost energy efficiency. The KWS network architecture comprises a Δ Input layer, a Δ Gated Recurrent Unit (Δ GRU) for the hidden layer, and a final fully-connected (FC) layer that classifies 12 GSCD classes.

The Δ RNN hardware accelerator is illustrated in Fig. 3. It features a Δ Encoder for calculating temporal differences of both the input activations ($\Delta x = x_t - x_{t-1}$) and hidden states ($\Delta h = h_t - h_{t-1}$), focusing on critical neuron updates that exceed the set delta threshold (Δ_{TH}) to optimize the trade-off between accuracy and energy consumption. The accelerator broadcasts each non-zero delta state to all delta FIFOs (Δ FIFOs) and utilizes eight multiply-accumulate (MAC) units for matrix-vector multiplication calculations. A State Assembler ensures proper update and coordination of Δ RNN states.

C. IIR BPF-based FEx

Fig. 4 describes the serial IIR BPF-based FEx [15] architecture generating 12b feature vectors to the Δ RNN accelerator. The FEx includes 1) a 4th-order IIR BPF, implemented as a cascade of two second-order sections (SOS), 2) a post-processing unit, which implements an envelope detector, channel-wise offset and scale adjustments, log compression, and normalization, 3) register files storing intermediate results and filter coefficients, and 4) a reconfiguration control module to select the channels for processing. The input GSCD speech samples are quantized to 12b and sub-sampled at 8 kHz before they are presented to the FEx.

1) Reduced Arithmetic Complexity in IIR BPF Design:

Fig. 5 shows the proposed low-arithmetic-complexity 4th order IIR BPF computation structure. According to the basic

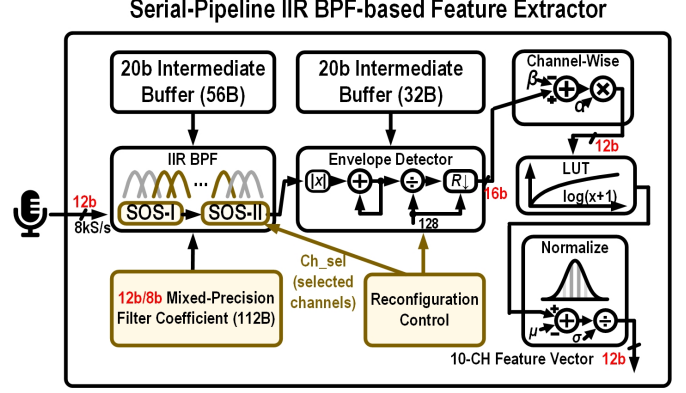


Fig. 4. The architecture of the serial time-domain IIR BPF-based FEx.

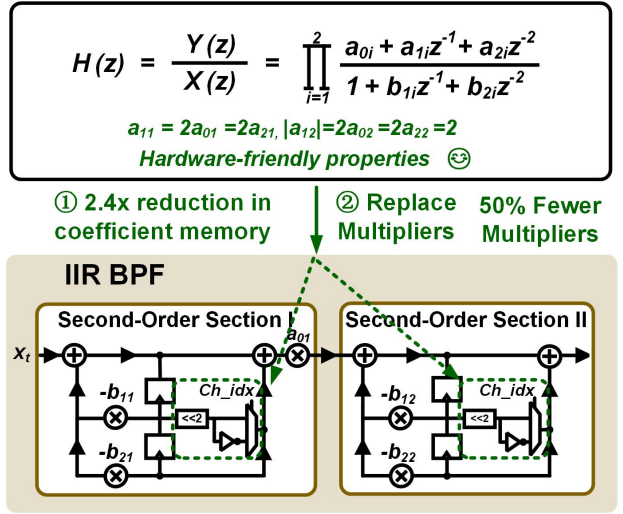


Fig. 5. Low arithmetic complexity structure of the 4th order IIR BPF.

architecture of a 4th order IIR BPF, 10 multipliers and 8 adders are required. If we look closer at coefficients a and b , we see hardware-friendly properties such as symmetries and constant value representations. By exploiting the hardware-friendly properties, half of the multipliers can be replaced with bit shifts.

2) *Reconfigurable Channel Selection*: The FEx is designed to be reconfigurable, supporting configurations from 1 to 16 channels. The simulated power versus KWS accuracy over different number of channels is shown in Fig. 6. The simulation results show that the 12-class KWS accuracy with GSCD is maintained even when the number of IIR filter channels decreases to 10 channels covering a frequency range from 516 Hz to 4.22 kHz. In the hardware design, the reconfiguration module adjusts the number of channels to be computed. In this case, selecting 10 channels instead of 16 reduces the power consumption of the FEx by 30%. In addition, the reconfigurable design enables our hardware to support up to 16 channels, providing flexibility for other applications that might benefit from a larger frequency range.

3) *Mixed-Precision Selection of Filter Coefficients*: Due to potential numerical stability issues, a fixed-point analysis is required during the IIR filter implementation. The selection of

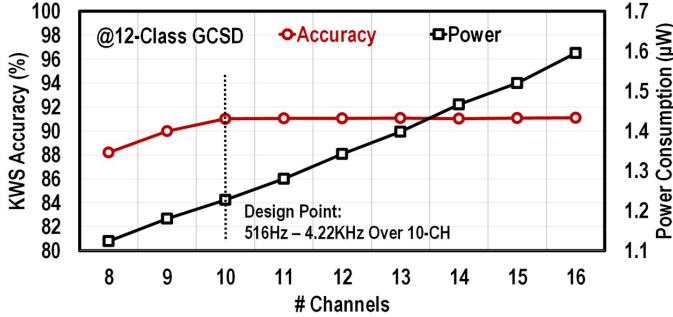


Fig. 6. Simulated power versus 12-class KWS accuracy over the different number of channels.

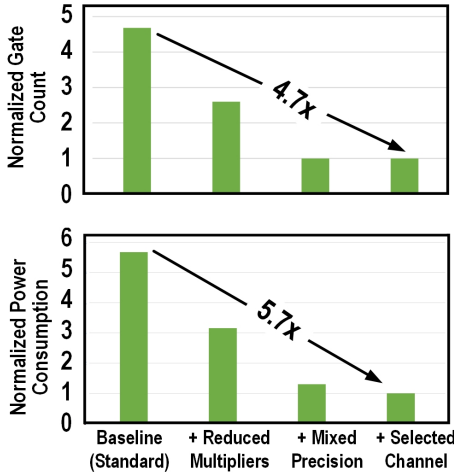


Fig. 7. The area (gate count) and power consumption optimization over each step.

coefficient precision is essential for power and area reduction. Previous works adopted the unified bit precision for coefficients. Thanks to the error resilience of neural networks, we can select an aggressive bit-width selection, in other words, the network accuracy is used as the measurement standard. Through a grid search, we find that the dynamic ranges for coefficients a and b across the filters of FEx are different, and the impact of bit precision on KWS accuracy also varies. The independent bit precision selection allows for further reduction of power and hardware resources. The integer bits for a and b are first determined separately using their maximum values. The fraction bits are then reduced from the baseline (16-bit) and the network accuracy is again quantified. From this optimization step, we find that 12b/8b (b/a) mixed precision is sufficient for the desired accuracy.

Fig. 7 depicts the power consumption and area (gate count) optimization over each optimization step. The filter coefficients are realized with 12b/8b mixed-precision, obtaining $2.4\times$ power and $2.6\times$ area reduction. Furthermore, the hardware-friendly properties (i.e., equivalence) of a and b coefficients of biquad filters are exploited so that half of the multipliers can be replaced with bit shifts, leading to $1.8\times$ power and $1.8\times$ area reduction. Putting them all together, the power and area of the proposed digital FEx are reduced by $5.7\times$ and $4.7\times$, respectively.

Unlike most prior arts [2], [16], [17] relying on 16b high-resolution analog-to-digital converters (ADCs), the proposed IIR digital FEx features a 12b-quantized audio signal, facilitating the usage of low-power/low-area 12b ADCs.

D. Near- V_{TH} Weight SRAM

Fig. 8 illustrates a 24kB weight SRAM operating at the 0.6 V near- V_{TH} voltage, which is divided into 12 banks of 2kB units each. The SRAM comprises 4 blocks (BLKs) of memory, a 10b address (A) register, a 16b input (D) register, a 0.6 V-to-0.65 V output (Q) level shifter for Δ RNN interfacing, and a skew-resistant column MUX. Note that the 0.6 V/0.65 V dual-supply approach was chosen only due to the low-to-high nature of I/O level shifter [18]. While not addressed in the design phase of this chip, a single supply operation is possible if the Q output bypasses I/O level shifters or by adopting a bidirectional level shifter [19]. The proposed SRAM deploys pitch-matched 6T level shifters that align with the 8T bitcell’s vertical pitch to convert word lines (WL/RWL) from 0.6 V to 1.2 V leading to enhanced access time and static noise margin.

Unlike prior art [20] relying on additional off-chip above- V_{DD} WL booster, the proposed SRAM features an on-chip-integrated voltage booster (V_{DDH}) [21]. Our combination approach of pitch-matched level shifter and voltage booster is distinct from [21], which utilized the booster circuit only for driving the footer of the read-buffer within the 8T bitcell, rather than word lines.

The SRAM operates at reduced leakage power by employing high- V_{TH} devices for bitcells. The column MUX uses dynamic NOR logic [22] and the proposed clock-skew-robust pre-charging scheme (PCHCMX), ensuring output data (Q) refreshes at the falling clock edge and facilitating easier integration of full-custom design with synthesized logic. The implemented full-custom SRAM achieves a $6.6\times$ lower read power of $0.93\ \mu\text{W}$ (only 18% of the total power of the chip) and a $2\times$ larger area than the push-rule foundry SRAM [23].

III. MEASUREMENT RESULTS

The die photo and measurement setup of the DeltaKWS chip fabricated in a 65 nm CMOS technology are shown in Fig. 9. Fig. 10 summarizes the power and area breakdown at 125 kHz operating frequency. The KWS chip consumes $5.22\ \mu\text{W}$. The IIR BPF-based FEx, Δ RNN accelerator, and near- V_{TH} SRAM consume 11%, 41%, and 48% of the total power, respectively. The IIR BPF-based FEx, Δ RNN accelerator, and near- V_{TH} SRAM consume 25%, 57%, and 18% of the total power, respectively. The chip core area is $0.78\ \text{mm}^2$. A MiniZed development board with a Xilinx Zynq 7007S SoC FPGA is used as a host to initialize and feed inputs to the KWS IC. To validate the KWS chip’s performance, we downsample the test GSCD audio streams to 8 kHz. The downsampling induces a negligible influence on the GSCD accuracy.

A. KWS Accuracy, Energy, and Latency

Fig. 11 shows the audio waveform of a 1-second GSCD “Yes” keyword and the measurement results on IIR features

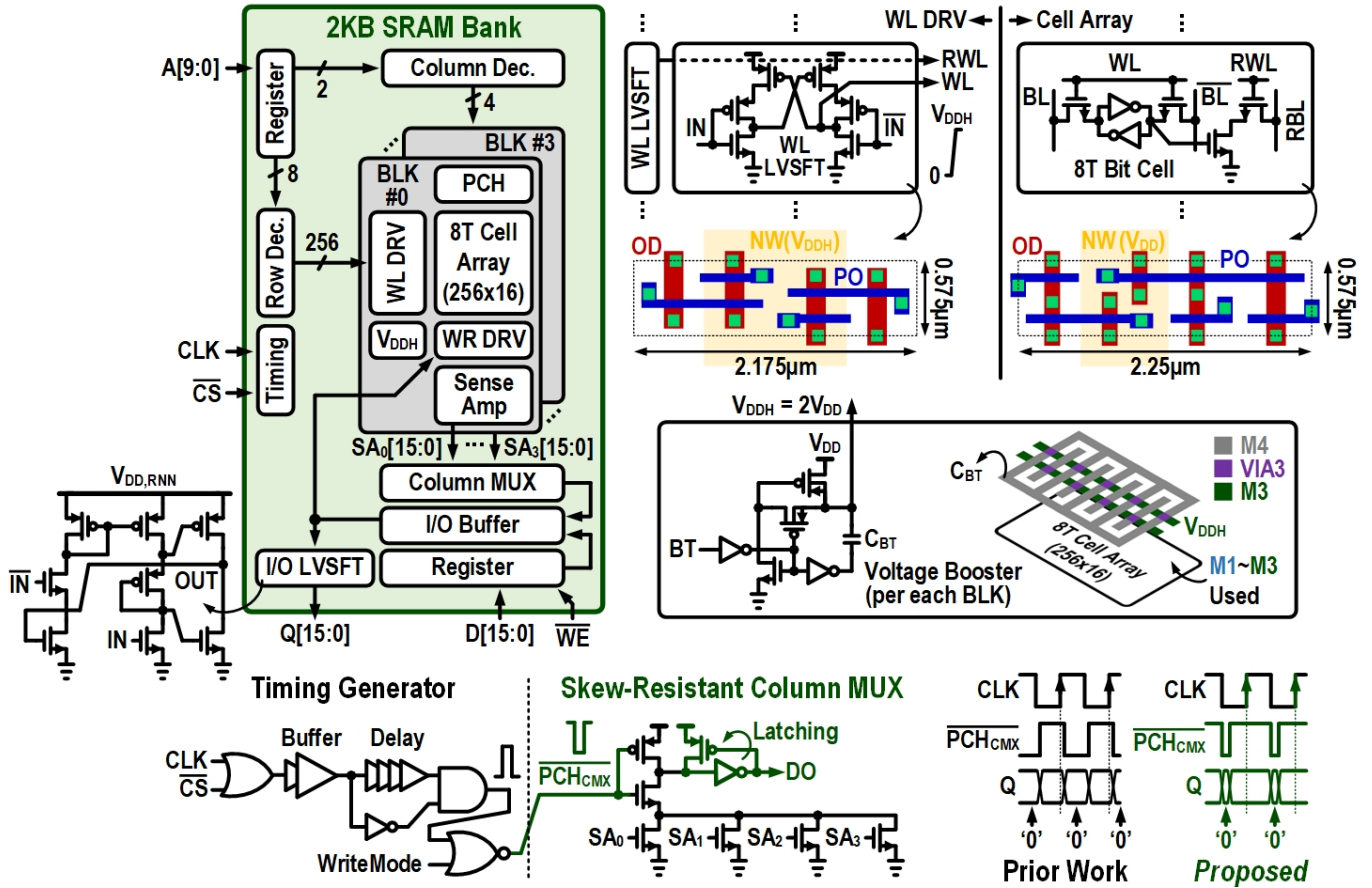


Fig. 8. 0.6V near- V_{TH} full-custom SRAM with pitch-matched WL level shifter, I/O level shifter, integrated voltage booster, timing generator, and skew-resistant column MUX.

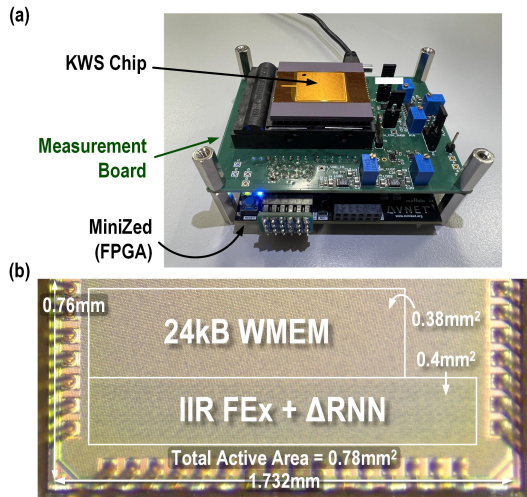


Fig. 9. (a) Measurement setup of the KWS chip. (b) Chip micrograph.

and the Δ RNN latency. The FEx produces 12-bit 10-channel features from IIR BPFs with Mel-scale center frequencies from 516 Hz to 4.22 kHz, that are fed to the Δ RNN accelerator through an asynchronous FIFO. Relatively silent frames in the “Yes” sample lead to around 40% latency reduction compared to active frames.

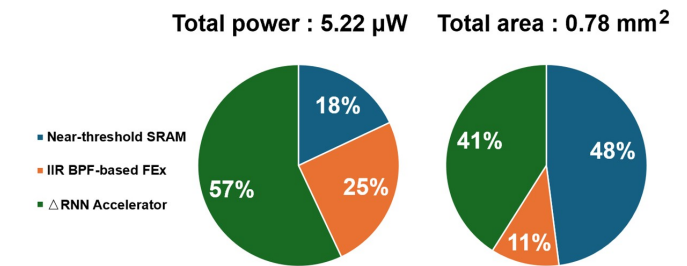


Fig. 10. Measured power and area breakdown of the KWS chip.

The temporal sparsity in the Δ RNN can be adjusted through Δ_{TH} . The level of sparsity also impacts the task accuracy; and the network energy and latency per input sample. Fig. 12 shows the measured 12-class GSCD KWS accuracy, energy per decision, average temporal sparsity and computing latency of the KWS chip at various Δ_{TH} . In comparison to $\Delta_{TH} = 0$, Δ_{TH} can be increased to 0.2 to achieve 87% temporal sparsity while maintaining 89.5% accuracy on the 12-class GSCD (less than 0.6% accuracy drop). At this Δ_{TH} value, the latency is reduced by $2.4\times$ to 6.9 ms and energy consumption by $3.4\times$ to 36.11 nJ/Decision.

These measurements were taken with the Δ RNN operating at a clock frequency of 125 kHz. This highlights the potential

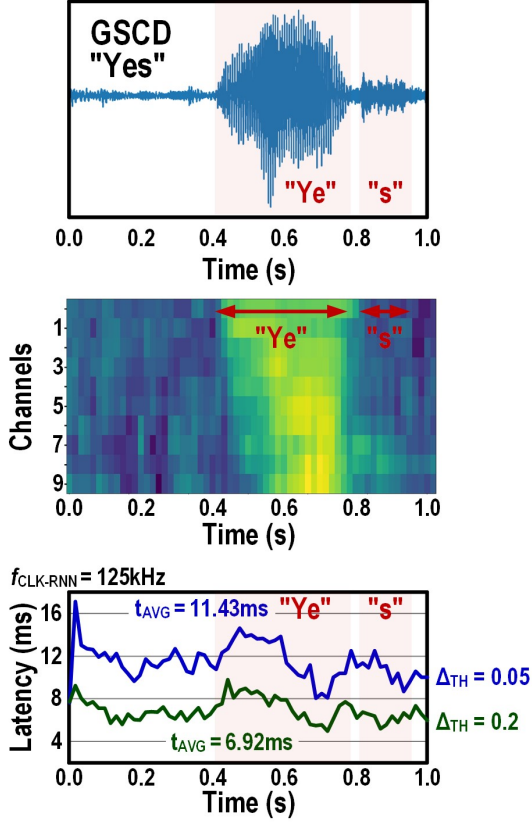


Fig. 11. (Top) audio waveform of “Yes” sample; (middle) measured IIR features and (bottom) Δ RNN latency for two Δ_{TH} values.

for significant energy savings in KWS applications through the optimization of Δ_{TH} . The measured SRAM waveform (Fig. 13) shows that the skew-resistant pre-charging scheme ensures Q data is always updated near the falling clock edge.

B. Comparison With SoTA Works

Table I compares the FEx of our KWS chip with other digital FEx implementations [2], [4]. Our 65 nm 12-bit digital serial IIR BPF-based FEx occupies an area of 0.084 mm², which is only 1.5 \times larger than the 28 nm 8-bit digital serial FFT-based Mel Frequency Cepstral Coefficients (MFCC) FEx (0.057 mm²) [2]. Despite the slightly larger area, our FEx provides 2 \times larger feature dimensions (channels) and consumes only 1.22 μ W. It also achieves a 5.9 \times reduction in power consumption compared to a previous 65 nm MFCC FEx [4], which also has lower feature precision (8-bit) compared to our 12-bit implementation.

Table II compares our KWS chip with other implementations [5], [8], [23]–[25]. Kim et al. [23] proposed a ring-oscillator-based time-domain FEx for better technology scalability, however, their KWS consumed 23 μ W power and achieved a limited 86.03% accuracy for 10-keyword KWS. Kosuge et al. [5] proposed a single-chip, fully synthesizable wired-logic DNN processor that achieved 88% accuracy for 10-keyword KWS with a latency of only 1.2 ms. However, the area of their chip is nearly 10 \times larger than our chip. Tan et al. [25] presented a low-power KWS chip also with

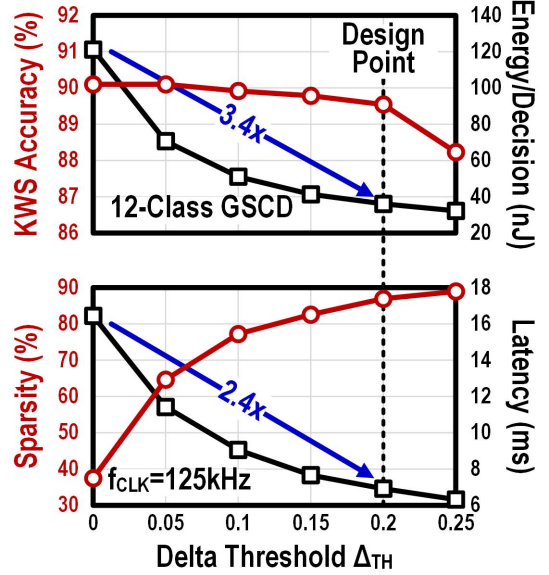


Fig. 12. Measured 12-class GSCD KWS accuracy, energy per decision, average temporal sparsity and computing latency at different delta thresholds Δ_{TH} . 125kHz clock is used. $\Delta_{TH} = 0.2$ is chosen as the design point, with 3.4x lower energy and 2.4x shorter latency at 87% sparsity.

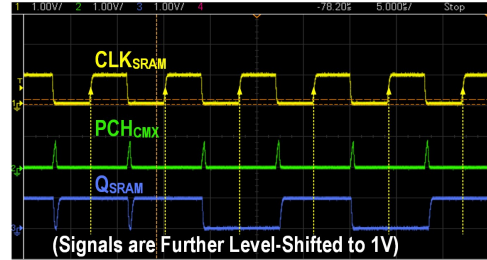


Fig. 13. Skew-resistant column MUX measurement from SRAM.

a low decision latency of just 2 ms, featuring a scalable 5T-SRAM. Frenkel et al. [24] proposed a spiking recurrent neural network processor that offers lower latency, however, it demonstrated results from only a single-keyword KWS. Seol et al. [8] presented a 1.5 μ W end-to-end KWS SoC, for only a 5-keyword KWS. These two works [8], [24] were limited to simpler tasks involving the classification of only a few keywords.

IV. CONCLUSION

This paper presented a KWS chip featuring a fine-grained temporary sparsity-aware Δ RNN accelerator, a compact IIR BPF-based FEx, and a low-power near- V_{TH} SRAM. With such techniques, our KWS chip, fabricated in a 65 nm CMOS process, achieves an energy consumption of 36 nJ/decision with a classification accuracy of 90.5%/89.5% on the 11-class/12-class GSCD dataset, respectively. The bio-inspired Δ RNN accelerator leveraging temporal similarities between neighboring feature vectors extracted from input frames and network hidden states, eliminating unnecessary operations and memory accesses, achieving 2.4 \times latency reduction and 3.4 \times energy per decision reduction. The serial IIR-BPF FEx that features

TABLE I
COMPARISON OF DIGITAL FEX. IMPLEMENTATIONS

Digital FEx.	Shan ISSCC'20 [2]	Giraldo JSSC'20 [4]	Shan JSSC'23 [16]	This Work
Process (nm)	28	65	28	65
Area (mm ²)	0.057	0.66	0.093	0.084
Clock (Hz)	40k	250k	8k	128k
Input Precision	16 bits	10 bits ^A	16 bits	12 bits
Feature Precision	8 bits	8 bits	8 bits	12 bits
Feature Type	MFCC	MFCC	MFCC	IIR
Feature Dimension	8	≤ 32	11	≤ 16
Backbone	256-point FFT	512-point FFT	128-point FFT	IIR-BPF
Data Storage (bytes)	256 ^D	-	512 ^D	200
Freq. Range (Hz)	16-8k	≤ 8k	≤ 4k	100-7.9k
Supply (V)	0.41	0.6/0.8	0.4	0.65
Power (μW)	0.34	7.2 ^B	0.17	1.22 ^C
Frame Shift (ms)	16	16	32	16
Frame Window Length (ms)	32	32	32	16
Serial FEx.	Yes	No	Yes	Yes

^A On-chip ADC ^B Measured with 13-D features ^C Measured with 10-D features
^D Data storage for just FFT module

TABLE II
COMPARISON OF KWS IMPLEMENTATIONS

KWS Refs	Kim ISSCC'22 [23]	Frenkel ISSCC'22 [24]	Seol ISSCC'23 [8]	Kosuge VLSI'23 [5]	Tan ISSCC'24 [25]	This Work	
Process (nm)	65	28	28	40	28	65	
Supply (V)	0.5/0.75	0.5	1.4/0.65/0.5	0.5	0.35/0.9	0.6/0.65	
Area (mm ²)	2.03	0.45	0.8	7.63	0.121	0.78	
On-Chip Memory (kB)	27	138	18	0	16	26.3	
Clock (Hz)	250k	13M	1M	120k	1M	125k	
Feature Ex.	Analog Time	-	Digital Freq.	TCN	TCN	Digital Time	
Algorithm	RNN	Spiking RNN	Skip RNN	CNN	Transfer Computing	ΔGRU-FC	
						Δ _{TH} = 0	Δ _{TH} = 0.2
Energy/Decision (nJ)	285.20	42	23.68	183.4	1.73	121.2	36.11
Comp. Latency (ms)	12.4	5.7	16	1.2	2	16.4	6.9
KWS Power (μW)	23 ^A	79	1.48 ^A	152.8	1.73	7.36	5.22
Dataset	GSCD	SHD ^B	GSCD	GSCD	GSCD	GSCD	
# Classes (# Keywords)	12 (10)	2 (1)	7 (5)	35 (35) 10 (10)	12 (10)	11 (10) / 12 (10)	
Accuracy (%)	86.03	90.7	92.8	78.2 88.0	91.8	91.1 / 90.1	90.5 / 89.5

^A Power includes AFE, FE, and NN. ^B Spiking Heidelberg Digits.

mixed-precision quantization, low-cost computing structure, and channel selection; achieving 5.7× power reduction and 4.7× area reduction. The 24 kB 0.6 V near-threshold-operating full-custom SRAM achieves 6.6× lower power consumption compared to the foundry-provided SRAM. The proposed KWS chip, incorporating an IIR BPF-based FEx, ΔRNN accelerator, and 24 kB near-threshold SRAM, occupies 0.78 mm².

ACKNOWLEDGMENT

The authors would like to thank Dr. Jinsu Lee, who was with KAIST, for the valuable feedback on the full-custom SRAM design, and Harim Kim, who is with Samsung Electronics, for his technical support of running SPICE-based post-layout simulations in Cadence Virtuoso environment.

The authors acknowledge the Swiss National Science Foundation BRIDGE - Proof of Concept Project (40B1-0 213731) and CA-DNNEdge project (208227) for partial funding of this work.

REFERENCES

- [1] K. Kim, C. Gao, R. Graça, I. Kiselev, H.-J. Yoo, T. Delbruck, and S.-C. Liu, "A 23-μW Keyword Spotting IC With Ring-Oscillator-Based Time-Domain Feature Extraction," *IEEE Journal of Solid-State Circuits*, vol. 57, no. 11, pp. 3298–3311, 2022.
- [2] W. Shan, M. Yang, J. Xu, Y. Lu, S. Zhang, T. Wang, J. Yang, L. Shi, and M. Seok, "A 510nW 0.41V Low-Memory Low-Computation Keyword-Spotting Chip Using Serial FFT-Based MFCC and Binarized Depthwise Separable Convolutional Neural Network in 28nm CMOS," in *IEEE International Solid-State Circuits Conference - (ISSCC)*, 2020, pp. 230–232.
- [3] H. Dbouk, S. K. Gonugondla, C. Sakr, and N. R. Shanbhag, "A 0.44-μJ/dec, 39.9-μs/dec, Recurrent Attention In-Memory Processor for Keyword Spotting," *IEEE Journal of Solid-State Circuits*, vol. 56, no. 7, pp. 2234–2244, 2021.
- [4] J. S. P. Giraldo, S. Lauwereins, K. Badami, and M. Verhelst, "Vocell: A 65-nm Speech-Triggered Wake-Up SoC for 10-μ W Keyword Spotting and Speaker Spotting," *IEEE Journal of Solid-State Circuits*, vol. 55, no. 4, pp. 868–878, 2020.
- [5] A. Kosuge, R. Sumikawa, Y.-C. Hsu, K. Shiba, M. Hamada, and T. Kuroda, "A 183.4nJ/inference 152.8μW Single-Chip Fully Synthesizable Wired-Logic DNN Processor for Always-On 35 Voice Commands

- Recognition Application,” in *IEEE Symposium on VLSI Technology and Circuits (VLSI Technology and Circuits)*, 2023, pp. 1–2.
- [6] F. Tan, W.-H. Yu, K.-F. Un, R. P. Martins, and P.-I. Mak, “A 0.05-mm² 2.91-nJ/Decision Keyword-Spotting (KWS) Chip Featuring an Always-Retention 5T-SRAM in 28-nm CMOS,” *IEEE Journal of Solid-State Circuits*, 2023.
- [7] C. Li, H. Zhi, K. Yang, J. Qian, Z. Yan, L. Zhu, C. Chen, X. Wang, and W. Shan, “A 0.61- μ W Fully Integrated Keyword-Spotting ASIC With Real-Point Serial FFT-Based MFCC and Temporal Depthwise Separable CNN,” *IEEE Journal of Solid-State Circuits*, vol. 59, no. 3, pp. 867–877, 2024.
- [8] J.-H. Seol, H. Yang, R. Rothe, Z. Fan, Q. Zhang, H.-S. Kim, D. Blaauw, and D. Sylvester, “A 1.5 μ W End-to-End Keyword Spotting SoC with Content-Adaptive Frame Sub-Sampling and Fast-Settling Analog Frontend,” in *IEEE International Solid-State Circuits Conference (ISSCC)*, 2023, pp. 1–3.
- [9] M. Horowitz, “1.1 computing’s energy problem (and what we can do about it),” in *2014 IEEE International Solid-State Circuits Conference Digest of Technical Papers (ISSCC)*, 2014, pp. 10–14.
- [10] D. Neil, J. H. Lee, T. Delbruck, and S.-C. Liu, “Delta Networks for Optimized Recurrent Network Computation,” in *Proceedings of the 34th International Conference on Machine Learning*, ser. Proceedings of Machine Learning Research, D. Precup and Y. W. Teh, Eds., vol. 70. PMLR, 06–11 Aug 2017, pp. 2584–2593.
- [11] C. Gao, D. Neil, E. Ceolini, S.-C. Liu, and T. Delbruck, “DeltaRNN: A Power-efficient Recurrent Neural Network Accelerator,” in *Proceedings of the 2018 ACM/SIGDA International Symposium on Field-Programmable Gate Arrays*, ser. FPGA ’18. New York, NY, USA: Association for Computing Machinery, 2018, p. 21–30. [Online]. Available: <https://doi.org/10.1145/3174243.3174261>
- [12] C. Gao, A. Rios-Navarro, X. Chen, S.-C. Liu, and T. Delbruck, “EdgeDRNN: Recurrent Neural Network Accelerator for Edge Inference,” *IEEE Journal on Emerging and Selected Topics in Circuits and Systems*, vol. 10, no. 4, pp. 419–432, 2020.
- [13] S.-C. Liu, C. Gao, K. Kim, and T. Delbruck, “Energy-efficient Activity-driven Computing Architectures for Edge Intelligence,” in *2022 International Electron Devices Meeting (IEDM)*, 2022, pp. 21.2.1–21.2.4.
- [14] F. Ottati, C. Gao, Q. Chen, G. Brignone, M. R. Casu, J. K. Eshraghian, and L. Lavagno, “To Spike or Not to Spike: A Digital Hardware Perspective on Deep Learning Acceleration,” *IEEE Journal on Emerging and Selected Topics in Circuits and Systems*, vol. 13, no. 4, pp. 1015–1025, 2023.
- [15] Q. Chen, Y. Chang, K. Kim, C. Gao, and S.-C. Liu, “An Area-Efficient Ultra-Low-Power Time-Domain Feature Extractor for Edge Keyword Spotting,” in *2023 IEEE International Symposium on Circuits and Systems (ISCAS)*, 2023, pp. 1–5.
- [16] W. Shan, J. Qian, L. Zhu, J. Yang, C. Huang, and H. Cai, “AAD-KWS: A Sub- μ W Keyword Spotting Chip With an Acoustic Activity Detector Embedded in MFCC and a Tunable Detection Window in 28-nm CMOS,” *IEEE Journal of Solid-State Circuits*, vol. 58, no. 3, pp. 867–876, 2023.
- [17] S. Zheng, P. Ouyang, D. Song, X. Li, L. Liu, S. Wei, and S. Yin, “An Ultra-Low Power Binarized Convolutional Neural Network-Based Speech Recognition Processor With On-Chip Self-Learning,” *IEEE Transactions on Circuits and Systems I: Regular Papers*, vol. 66, no. 12, pp. 4648–4661, Dec. 2019.
- [18] R. Lotfi, M. Saberi, S. R. Hosseini, A. R. Ahmadi-Mehr, and R. B. Staszewski, “Energy-Efficient Wide-Range Voltage Level Shifters Reaching 4.2 fJ/Transition,” *IEEE Solid-State Circuits Letters*, vol. 1, no. 2, pp. 34–37, 2018.
- [19] S.-C. Luo, C.-J. Huang, and Y.-H. Chu, “A Wide-Range Level Shifter Using a Modified Wilson Current Mirror Hybrid Buffer,” *IEEE Transactions on Circuits and Systems I: Regular Papers*, vol. 61, no. 6, pp. 1656–1665, 2014.
- [20] I. J. Chang, J.-J. Kim, S. P. Park, and K. Roy, “A 32kb 10T Subthreshold SRAM Array with Bit-Interleaving and Differential Read Scheme in 90nm CMOS,” in *2008 IEEE International Solid-State Circuits Conference - Digest of Technical Papers*, 2008, pp. 388–622.
- [21] N. Verma and A. P. Chandrakasan, “A 65nm 8T Sub-Vt SRAM Employing Sense-Amplifier Redundancy,” in *2007 IEEE International Solid-State Circuits Conference. Digest of Technical Papers*, 2007, pp. 328–606.
- [22] S. Gupta, K. Gupta, B. H. Calhoun, and N. Pandey, “Low-Power Near-Threshold 10T SRAM Bit Cells With Enhanced Data-Independent Read Port Leakage for Array Augmentation in 32-nm CMOS,” *IEEE Transactions on Circuits and Systems I: Regular Papers*, vol. 66, no. 3, pp. 978–988, 2019.
- [23] K. Kim, C. Gao, R. Graça, I. Kiselev, H.-J. Yoo, T. Delbruck, and S.-C. Liu, “A 23 μ W Solar-Powered Keyword-Spotting ASIC with Ring-Oscillator-Based Time-Domain Feature Extraction,” in *2022 IEEE International Solid-State Circuits Conference (ISSCC)*, vol. 65, 2022, pp. 1–3.
- [24] C. Frenkel and G. Indiveri, “ReckOn: A 28nm Sub-mm² Task-Agnostic Spiking Recurrent Neural Network Processor Enabling On-Chip Learning over Second-Long Timescales,” in *2022 IEEE International Solid-State Circuits Conference (ISSCC)*, vol. 65, 2022, pp. 1–3.
- [25] F. Tan, W.-H. Yu, J. Lin, K.-F. Un, R. P. Martins, and P.-I. Mak, “A 1.8% FAR, 2ms Decision Latency, 1.73 nJ/Decision Keywords Spotting (KWS) Chip Incorporating Transfer-Computing Speaker Verification, Hybrid-Domain Computing and Scalable 5T-SRAM,” in *IEEE International Solid-State Circuits Conference (ISSCC)*, vol. 67. IEEE, 2024, pp. 330–332.

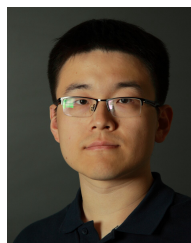


Qinyu Chen (Member, IEEE) is an Assistant Professor at the Leiden Institute of Advanced Computer Science (LIACS), Leiden University, Leiden, the Netherlands. She received the Ph.D. degree in Electronic Science and Technology from Nanjing University, Nanjing, China, in 2021. She was a visiting student from 2019 to 2020, and a Postdoctoral Researcher from 2022 to 2024, at the Institute of Neuroinformatics, University of Zürich and ETH Zürich, Zurich, Switzerland. Her current research interest includes the seamless brain-inspired AI system at the edge, and its application in healthcare, AR/VR with a focus on event-based processing. In 2022, She received a Bridge Fellowship Grant from the Swiss National Science Foundation (SNSF) and Innosuisse. She also serves as a member of the Neural Systems and Applications (NSA) Technical Committee in the IEEE Circuit and System Society (CASS).



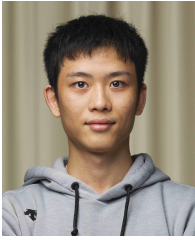
Kwantae Kim (Member, IEEE) received the B.S., M.S., and Ph.D. degrees in the School of Electrical Engineering from KAIST, South Korea, in 2015, 2017, and 2021, respectively. He is an Assistant Professor at the Department of Electronics and Nanoengineering, School of Electrical Engineering, Aalto University, Finland.

From 2015 to 2017, he was also with Healthrian R&D Center, South Korea, where he designed analog readout ICs for mobile healthcare solutions. He was a Visiting Student in 2020, and a Postdoctoral Researcher from 2021 to 2023, at the Institute of Neuroinformatics, University of Zurich and ETH Zurich, and an Established Researcher from 2023 to 2024, at the Department of Information Technology and Electrical Engineering (D-ITET), ETH Zurich, Switzerland. His research interests include analog/mixed-signal ICs and full-custom memory ICs for neuromorphic signal processing, biomedical sensors, and in-memory computing.



Chang Gao (Member, IEEE) received his Ph.D. degree with Distinction in Neuroscience from the Institute of Neuroinformatics, University of Zürich and ETH Zürich, Zürich, Switzerland, in March 2022. In August 2022, he joined the Delft University of Technology, The Netherlands, as an Assistant Professor in the Department of Microelectronics. He received the 2022 Misha Mahowald Early Career Award in Neuromorphic Engineering, the 2022 Marie-Curie Postdoctoral Fellowship, and the title of 2023 MIT Technology Review Innovators Under 35

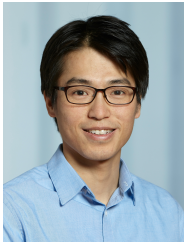
in Europe for his contribution to algorithm-hardware co-design for efficient sparse recurrent neural network edge computing. His current research interest is in developing digital AI hardware accelerators and their applications in future wireless communications, video/audio processing, healthcare, and robotics.



Sheng Zhou (Graduate Student Member, IEEE) received his bachelor's degree in computer science from the Hong Kong University of Science and Technology, and master's degree in data science from ETH Zurich. He is currently pursuing the Ph.D. degree in the Sensors Group at the Institute of Neuroinformatics, University of Zurich and ETH Zurich. His research interest is in mixed-signal circuit design for ultra-low-power edge applications.



Shih-Chii Liu (Fellow, IEEE) received the bachelor's degree in electrical engineering from the Massachusetts Institute of Technology, Cambridge, MA, USA, and the Ph.D. degree in the Computation and Neural Systems program from the California Institute of Technology, Pasadena, CA, USA, in 1997. She is currently Adjunct Professor in the Faculty of Science at the University of Zurich. She co-directs the Sensors group at the Institute of Neuroinformatics, University of Zurich and ETH Zurich. Her group's research focuses on sensor integrated circuit designs including the spiking silicon cochlea and bio-inspired auditory sensors; and real-time energy-efficient hardware systems that combine both sensor and event-driven low-compute deep neural network algorithms, targeting always-on edge AI and wearable applications.



Taekwang Jang (Senior Member, IEEE) received his B.S. and M.S. in electrical engineering from KAIST, Korea, in 2006 and 2008, respectively. From 2008 to 2013, he worked at Samsung Electronics Company Ltd., Yongin, Korea, focusing on mixed-signal circuit design, including analog and all-digital phase-locked loops for communication systems and mobile processors. In 2017, he received his Ph.D. from the University of Michigan and worked as a post-doctoral research fellow at the same institution. In 2018, he joined ETH Zürich as an assistant

professor and is leading the Energy-Efficient Circuits and Intelligent Systems group. He is also a member of the Competence Center for Rehabilitation Engineering and Science, and the chair of the IEEE Solid-State Circuits Society, Switzerland chapter.

His research focuses on circuits and systems for highly energy-constrained applications such as wireless sensor nodes and biomedical interfaces. Essential building blocks such as a sensor interface, energy harvester, power converter, communication transceiver, frequency synthesizer, and data converters are his primary interests. He holds 15 patents and has (co)authored more than 80 peer-reviewed conferences and journal articles. He is the recipient of the 2024 IEEE Solid-State Circuits Society New Frontier Award, the SNSF Starting Grant, the IEEE ISSCC 2021 and 2022 Jan Van Vessel Award for Outstanding European Paper, the IEEE ISSCC 2022 Outstanding Forum Speaker Award, and the 2009 IEEE CAS Guillemin-Cauer Best Paper Award. Since 2022, he has been a TPC member of the IEEE International Solid-State Circuits Conference (ISSCC), IMD Subcommittee, and IEEE Asian Solid-State Circuits Conference (ASSCC), Analog Subcommittee. He also chaired the 2022 IEEE International Symposium on Radio-Frequency Integration Technology (RFIT), Frequency Generation Subcommittee. Since 2023, he has been serving as an Associate Editor for the Journal of Solid-State Circuits (JSSC) and was appointed as a Distinguished Lecturer for the Solid-State Circuits Society in 2024.



Tobi Delbruck (Fellow, IEEE) received the degree in physics from University of California in 1986 and Ph.D. degree from Caltech in 1993. Currently, he is a Professor of Physics and Electrical Engineering at the Institute of Neuroinformatics, University of Zurich and ETH Zurich, where he has been since 1998. He co-directs the Sensors group, and his current research focus is on neuromorphic sensory processing, control, and efficient hardware AI.